The effect of cooling during deformation on recrystallized grain size piezometry

Hamid Soleymani[1*], Steven Kidder[2], Greg Hirth[3], Gordana Garapić[4]

[1]*Department of Earth and Environmental Sciences, The Graduate Center, CUNY; 365 5th Ave, New York, NY 10016*
[2]*Department of Earth and Atmospheric Sciences, City College of New York, CUNY; 160 Convent Ave, New York, NY 10031*
[3]*Department of Earth, Environmental, and Planetary Sciences, Brown University; 324 Brook St, Providence, RI 02912*
[4]*Department of Geology, State University of New York at New Paltz, 1 Hawk Dr, New Paltz, NY 12561*

ABSTRACT

Most exposed middle- and lower-crustal shear zones experienced deformation while cooling. We investigate the effect of the strengthening associated with such cooling on differential stress estimates based on recrystallized grain size. Typical geologic ratios of temperature-change-per-strain-unit were applied in Griggs Rig general shear experiments on quartzite with cooling rates between 2 to 10 °C/hr from 900 to 800 °C, and a shear strain rate of $\sim 2\times10^{-5}$ s^{-1}. Comparisons between these "cooling-ramp" experiments and control experiments at constant temperatures of 800 and 900 °C indicate that recrystallized grain size does not "keep pace" with evolving stress. Mean recrystallized grain sizes of the cooling-ramp experiments are twice as large as expected from the final stresses of the experiments. The traditional approach to piezometry involves a routine assumption of a steady-state microstructure, and would underestimate the final stress during the cooling-ramp experiments by $\sim 40\%$. Recrystallized grain size in the cooling-ramp experiments is a better indicator of the average stress of the experiments (shear strains ≥ 3). Due to the temperature sensitivity of recrystallization processes and rock strength, the results may

under-represent the effect of cooling in natural samples. Cooling-ramp experiments produce wider and more skewed grain size distributions than control experiments, suggesting that analyses of grain size distributions might be used to quantify the degree to which grain size departs from steady-state values due to cooling, and thereby provide more accurate constraints on final stress.

INTRODUCTION

The stress magnitude in the crust, and its spatial and temporal variability, remains an active research area in geodynamics, earthquake mechanics, structural geology, and rock mechanics (e.g., Kohlstedt et al., 1995). One of the most widely-used tools for quantifying stress magnitudes from middle crustal rock samples is recrystallized grain size piezometry (e.g., Twiss, 1977; Derby and Ashby, 1987; Shimizu, 1998; De Bresser et al., 2001). In laboratory experiments on quartz and other materials undergoing dislocation creep, there is a well characterized inverse relationship between differential stress (referred to below as "stress") and the size of new "dynamically recrystallized" grains produced during deformation (e.g., Fig. 1A). Experiments suggest that the relationship between flow stress and recrystallized grain size in quartz is independent of temperature, strain rate, and water content (Stipp et al., 2006). As currently implemented for geologic samples, for any mean recrystallized grain size, there is a single stress value that is assumed to represent some (unknown) final period of time when a rock was deformed at a relatively steady-state stress. Such stresses are often interpreted as representing peak stresses associated with ductile deformation near the brittle-ductile transition (e.g., Behr and Platt, 2011; Kidder et al., 2012). With the exception of samples strongly affected by seismic activity (e.g., Bestmann et al., 2012; Trepmann and Seybold, 2019), or subject to post-deformation annealing (e.g., Hacker et al., 1992), we are unaware of any significant previous evidence that supports or disproves this "steady-state" assumption. Hundreds of studies have used the recrystallized grain

size piezometer on various minerals and either implicitly or explicitly assumed that the recrystallized grain size populations being measured resulted from long-term, steady-state deformation (e.g., Twiss, 1977; Kohlstedt and Weathers, 1980; Hacker et al., 1992; Dunlap et al., 1997; Hirth et al., 2001; Behr and Platt, 2011; Kidder et al., 2012). We explored the validity of the steady-state assumption by carrying out experiments in which cooling was imposed during deformation. Since cooling strengthens rocks in the ductile regime, stress gradually increased during the experiments. Deformation conditions spanned a range of temperature change per strain unit typical of natural shear zones (Fig. 2).

EXPERIMENTS

All of the experiments were carried out in general shear on samples synthesized from silica gel following the routine of Nachlas (2016). Three cooling-ramp experiments and three constant-temperature control experiments were conducted to a shear strain (γ) of ~ 4 (Figs. 1A, B). One additional deformation experiment was carried out to a relatively small strain ($\gamma = 1.2$) at 900 °C. Another sample (not included in Table 1) was quenched following annealing. This undeformed sample exhibits a heterogeneous mixture of large (~ 100 μm) and small (~ 15 μm) grains (Fig. S1c). Stress vs. strain curves are shown in figure 1B. Shear strain rate ($\dot{\gamma}$) and confining pressure for all experiments were 2×10^{-5} s^{-1} and ~ 1.1 GPa, respectively. Control experiments were conducted at temperatures of 800 and 900 °C, or in the case of experiment (W2143), at 800 °C following deformation to $\gamma = 1.2$ at 900 °C (Fig. 1B). The experimental conditions at 900 °C fall near the previously determined boundary between dislocation creep regimes 2 and 3 (Hirth and Tullis, 1992), and at 800 °C, near the regime 1-2 boundary. Cooling-ramp experiments were conducted at a constant temperature of 900 °C prior to cooling. Cooling was imposed between temperatures of 900 and 800 °C at rates of 2, 4, and 10 °C/hr, and the initiation of the cooling was

timed so that a total strain of γ ≈ 4 was achieved when temperatures reached 800 °C (Fig. 1B). Thus, slow cooling-ramp samples experienced more strain during cooling. Electron Backscatter Diffraction (EBSD) maps with a step size of 0.15 or 0.2 µm were analyzed with MTEX (Hielscher and Schaeben, 2008). Recrystallized grains were identified using the routine of Cross et al. (2017). Additional information on methods, sample preparation, and EBSD processing are provided in the supplementary information.

RESULTS

Sample strengths fall at expected values given the experimental conditions. Final sample strengths for the control samples are similar to those predicted by the Hirth et al. (2001) flow law (Fig. 1A). The two control experiments deformed near the regime 1-2 boundary followed different stress-strain paths, but finished at a similar stress: sample W2136 deformed at a relatively constant stress typical of regime 2, while sample W2143 exhibited strain hardening then weakening as typical of regime 1. The cooling-ramp samples also experienced strain hardening, as indicated by higher final stress values relative to those of the control experiments (Table 1, Fig. 1B).

Initial microstructures at the onset of cooling are inferred from the samples deformed at 900 °C. The mean grain size (all grains) of the sample deformed to γ = 1.2 (W2112) is ~ 15 µm. Recrystallized grain size of the larger strain 900 °C experiment (W2142) is 7 µm, consistent with the piezometer (Fig. 1A). Both of these samples exhibit abundant subgrains and interlobate grain boundaries (Fig S2) as expected for samples deformed near the regime 2-3 boundary (Hirth and Tullis, 1992). The 800 °C control samples also have abundant subgrains, and grain boundaries marked by small-scale bulges (Fig S2). The cooling-ramp samples all show a range of microstructures associated with relatively low-temperature/higher stress deformation that are also

evident in the 800 °C control experiments, e.g., widespread bulges along grain boundaries, sweeping extinction, and deformation lamellae (Fig. S3).

Grain size and grain size distributions differ between the control and cooling-ramp experiments. Grain sizes (overall and recrystallized) of the cooling-ramp experiments correlate with the magnitude of cooling rate from values that grossly resemble the high strain 900 °C control experiment (10 and 4 °C/hr cooling rates), to values that resemble those of the 800 °C control experiments (2 °C/hr cooling rate; Table 1). In addition, the grain size distributions of the two fastest cooling-ramp samples (those furthest from "steady-state" in figure 2) are wider than the other experiments (Fig. 3). These larger grain size spreads are visually evident from grain outline maps (Fig. 3B) showing higher abundance of both coarse grains and fine grains for the faster cooling samples. Relative spread values, listed in Table 1, are quantified using the geometric coefficient of variation (GCV, Jensen et al., 2000), a size-independent measure of "standard deviation" of lognormally distributed data. GCV values increase with increased cooling rate; the value for the fastest cooling-ramp sample is 18% larger than the control experiment average. Nonparametric skew (NP skew = (mean-median)/stdev) is uniformly higher (~ 16%) in the cooling-ramp experiments relative to the controls. Standard skew values are heavily influenced by large outlier grains, but if outliers are removed (Tukey, 1981) and skew recalculated, the cooling-ramp experiments have the largest asymmetry by this measure (11-24% larger than control experiment average; Table 1).

Grain orientation spread (GOS), which measures distortion within grains, is also substantially higher in the cooling-ramp experiments (Table 1). Other microstructures, however, do not appear to discriminate between the two types of experiments. For example, aspect ratios are highest in the experiment with a cooling rate of 10 °C/hr, but are not elevated relative to control experiments in

the other cooling-ramp experiments, and intensity of lattice preferred orientation is similar between cooling-ramps and controls (Table 1).

DISCUSSION

Our results demonstrate that recrystallized grain size does not "keep pace" with increasing stress at deformation conditions scaled to the cooling rates of typical shear zones. Recrystallized grain sizes of the cooling-ramp experiments are nearly twice as large as would be predicted by the piezometer at final stress values (Fig. 1A). In turn, the final stresses of the experiments are ~ 40% larger than would be estimated based on traditional piezometry (Table 1).

These values may underestimate the true magnitude of the effect of cooling during deformation for natural samples because at colder conditions underlying Arrhenius relationships may dictate 1) slower rates of microstructural change, and 2) larger differences in steady-state recrystallized grain size. Grain size evolution models and experimental evidence indicate slower microstructural evolution rates at lower temperatures (e.g., Austin and Evans, 2009; Holtzman et al., 2018, Cross and Skemer, 2019). Additionally, owing to the Arrhenius relationship underlying the steady-state strength of quartz, a temperature change of 100 °C at geologic conditions corresponds with a larger percent change in steady-state recrystallized grain size than occurs in the laboratory (the change in 1/T due to a 100 °C shift is larger in the crust). Despite strain hardening in the ramp experiments, the relative shift required to maintain a steady-state grain size during a 100 °C temperature change is predicted to be roughly twice as large under natural conditions than in the cooling-ramp experiments (see supplementary material). Any strain hardening occurring in natural shear zones would further accentuate this difference. In summary, relative to higher-temperature laboratory conditions, we anticipate that in nature, greater microstructural changes are required to "keep pace" with a temperature change, while at the same time, mechanisms for

6

achieving such change are slowed. Such general predictions provide impetus for improving and applying grain size evolution models (e.g., Austin and Evans, 2009; Holtzman et al., 2018) and clarifying potential effects of temperature differences on steady-state grain size (De Bresser et al., 2001).

Conventional grain size piezometry is thus likely to underestimate peak stresses experienced by rocks exhumed through the brittle-ductile transition. Stresses calculated using the recrystallized grain size piezometer should be considered minimum constraints on the final stress associated with dynamic recrystallization, unless it can be determined that deformation occurred at a relatively constant temperature. Such underestimated stresses could explain the discrepancy noted by Behr and Platt (2011) in the Whipple Mountains between geologic constraints on strain rate and flow law predictions based on piezometry. Recrystallized grain size is a better indicator of the average stress of the entire experiments (Table 1) rather than peak stress.

Considering the likelihood that typical geologic rates of cooling and deformation significantly affect stress estimates from paleopiezometry, it is important, if possible, to distinguish microstructures formed under such conditions from those formed during steady-state flow. The results of our experiments suggest that the effects of cooling may be distinguished by wider and more asymmetric grain size distributions (Table 1, Fig. 3). This result can be intuitively understood in a simplified model wherein recrystallized grains have a piezometrically-stable size near the moment they form (e.g., Stipp et al., 2010; Kidder et al., 2012, 2016) and minimal growth occurs thereafter (e.g., Platt and de Bresser, 2017)—as increasingly smaller grains are generated over time, the left side of the grain size distribution will inflate, leading to a rightward skew and wider distribution (Table 1, Fig. 3A). We hypothesize that these patterns could be more pronounced in natural settings involving larger amounts of strain and cooling over a larger range of temperature.

If so, it might be possible to constrain the ratio of temperature change to strain rate (i.e., $dT/d\gamma$ contours in Fig. 2) from microstructural measurements. This could enable an estimate of peak stress by the application of some correction factor calibrated by experiments or predicted by modeling of grain size distributions (e.g., Piazolo et al., 2002). Where cooling rate is known, estimates of $dT/d\gamma$ from a rock's microstructure would allow an estimation of strain rate (Fig. 2)—a rheologically significant quantity that is even less-well constrained than stress (e.g., Fagereng and Biggs, 2018).

ACKNOWLEDGMENTS

REFERENCES CITED

Austin, N., and Evans, B., 2009, The kinetics of microstructural evolution during deformation of calcite: Journal of Geophysical Research: Solid Earth, v. 114, p. 1–22, doi:10.1029/2008JB006138.

Behr, W.M., and Platt, J.P., 2011, A naturally constrained stress profile through the middle crust in an extensional terrane: Earth and Planetary Science Letters, v. 303, p. 181–192, doi:10.1016/j.epsl.2010.11.044.

Bestmann, M., Pennacchioni, G., Nielsen, S., Göken, M., and De Wall, H., 2012, Deformation and ultrafine dynamic recrystallization of quartz in pseudotachylyte-bearing brittle faults: A matter of a few seconds: Journal of Structural Geology, v. 38, p. 21–38.

De Bresser, J.H.P., Ter Heege, J.H., and Spiers, C.J., 2001, Grain size reduction by dynamic

recrystallization: Can it result in major rheological weakening? International Journal of Earth Sciences, v. 90, p. 28–45, doi:10.1007/s005310000149.

Cross, A.J., Prior, D.J., Stipp, M., and Kidder, S., 2017, The recrystallized grain size piezometer for quartz: An EBSD-based calibration: Geophysical Research Letters, v. 44, p. 6667–6674, doi:10.1002/2017GL073836.

Cross, A.J., and Skemer, P., 2019, Rates of Dynamic Recrystallization in Geologic Materials: Journal of Geophysical Research: Solid Earth, doi:10.1029/2018jb016201.

Derby, B., and Ashby, M.F., 1987, On dynamic recrystallisation: Scripta Metallurgica, v. 21, p. 879–884.

Dunlap, W.J., Hirth, G., and Teyssier, C., 1997, Thermomechanical evolution of a ductile duplex: Tectonics, v. 16, p. 983–1000.

Fagereng, Å., and Biggs, J., 2018, New perspectives on ' geological strain rates ' calculated from both naturally deformed and actively deforming rocks: Journal of Structural Geology, p. 1–11, doi:10.1016/j.jsg.2018.10.004.

Foster, D.A., and John, B.E., 1999, Quantifying tectonic exhumation in an extensional orogen with thermochronology: examples from the southern Basin and Range Province: Geological Society, London, Special Publications, v. 154, p. 343–364, doi:10.1144/gsl.sp.1999.154.01.16.

Hacker, B.R., Yin, A., Christie, J.M., and Davis, G.A., 1992, Stress magnitude, strain rate, and rheology of extended middle continental crust inferred from quartz grain sizes in the Whipple Mountains, California: Tectonics, v. 11, p. 36–46.

Heilbronner, R., and Kilian, R., 2017, The grain size(s) of Black Hills Quartzite deformed in the dislocation creep regime: Solid Earth, v. 8, p. 1071–1093, doi:10.5194/se-8-1071-2017.

Hielscher, R., and Schaeben, H., 2008, research papers A novel pole figure inversion method : specification of the MTEX algorithm research papers: , p. 1024–1037, doi:10.1107/S0021889808030112.

Hirth, G., Teyssier, C., and Dunlap, J.W., 2001, An evaluation of quartzite flow laws based on comparisons between experimentally and naturally deformed rocks: International Journal of Earth Sciences, v. 90, p. 77–87, doi:10.1007/s005310000152.

Hirth, G., and Tullis, J., 1992, Dislocation creep regimes in quartz aggregates: Journal of Structural Geology, v. 14, p. 145–159, doi:10.1016/0191-8141(92)90053-Y.

Holtzman, B.K., Chrysochoos, A., and Daridon, L., 2018, A thermomechanical framework for analysis of microstructural evolution: Application to olivine rocks at high temperature: Journal of Geophysical Research: Solid Earth, v. 123, p. 8474–8507.

Jensen, J., Lake, L.W., Corbett, P.W.M., and Goggin, D., 2000, Statistics for petroleum engineers and geoscientists: Gulf Professional Publishing, v. 2.

Kidder, S., Avouac, J.P., and Chan, Y.C., 2013, Application of titanium-in-quartz thermobarometry to greenschist facies veins and recrystallized quartzites in the Hsüehshan range, Taiwan: Solid Earth, v. 4, p. 1–21, doi:10.5194/se-4-1-2013.

Kidder, S., Avouac, J.-P.P., and Chan, Y.-C.C., 2012, Constraints from rocks in the Taiwan orogen on crustal stress levels and rheology: Journal of Geophysical Research: Solid Earth, v. 117, p. 1–13, doi:10.1029/2012JB009303.

Kidder, S., Hirth, G., Avouac, J.-P., and Behr, W., 2016, The influence of stress history on the grain size and microstructure of experimentally deformed quartzite: Journal of Structural Geology, v. 83, p. 194–206, doi:10.1016/j.jsg.2015.12.004.

Kohlstedt, D.L., Evans, B., and Mackwell, S.J., 1995, Strength of the lithosphere: Constraints

imposed by laboratory experiments: Journal of Geophysical Research: Solid Earth, v. 100, p. 17587–17602, doi:10.1029/95jb01460.

Kohlstedt, D.L., and Weathers, M.S., 1980, Deformation-induced microstructures, paleopiezometers, and differential stresses in deeply eroded fault zones: Journal of Geophysical Research: Solid Earth, v. 85, p. 6269–6285.

Nachlas, W.O., 2016, Precise and Accurate Doping of Nanoporous Silica Gel for the Synthesis of Trace Element Microanalytical Reference Materials: Geostandards and Geoanalytical Research, v. 40, p. 505–516.

Norris, R.J., and Cooper, A.F., 2003, Very high strains recorded in mylonites along the Alpine Fault, New Zealand: implications for the deep structure of plate boundary faults: Journal of Structural Geology, v. 25, p. 2141–2157, doi:10.1016/s0191-8141(03)00045-2.

Paterson, M.S., and Olgaard, D.L., 2000, Rock deformation tests to large shear strains in torsion: Journal of Structural Geology, v. 22, p. 1341–1358, doi:10.1016/S0191-8141(00)00042-0.

Piazolo, S., Bons, P.D., Jessell, M.W., Evans, L., and Passchier, C.W., 2002, Dominance of microstructural processes and their effect on microstructural development: insights from numerical modelling of dynamic recrystallization: Geological Society, London, Special Publications, v. 200, p. 149–170.

Platt, J.P., and De Bresser, J.H.P., 2017, Stress dependence of microstructures in experimentally deformed calcite: Journal of Structural Geology, v. 105, p. 80–87.

Sassier, C., Leloup, P.-H.H., Rubatto, D., Galland, O., Yue, Y., and Lin, D., 2009, Direct measurement of strain rates in ductile shear zones: A new method based on syntectonic dikes: Journal of Geophysical Research: Solid Earth, v. 114, p. 1–22, doi:10.1029/2008JB005597.

Shimizu, I., 1998, Stress and temperature dependence of recrystallized grain size: a subgrain

misorientation model: Geophysical Research Letters, v. 25, p. 4237–4240.

Stipp, M., Fügenschuh, B., Gromet, L.P., Stünitz, H., and Schmid, S.M., 2004, Contemporaneous plutonism and strike-slip faulting: A case study from the Tonale fault zone north of the Adamello pluton (Italian Alps): Tectonics, v. 23, p. 1–23, doi:10.1029/2003TC001515.

Stipp, M., Tullis, J., and Behrens, H., 2006, Effect of water on the dislocation creep microstructure and flow stress of quartz and implications for the recrystallized grain size piezometer: Journal of Geophysical Research: Solid Earth, v. 111, p. 1–19, doi:10.1029/2005JB003852.

Stipp, M., Tullis, J., Scherwath, M., and Behrmann, J.H., 2010, A new perspective on paleopiezometry: Dynamically recrystallized grain size distributions indicate mechanism changes: Geology, v. 38, p. 759–762, doi:10.1130/g31162.1.

Stockli, D.F., Brichau, S., Dewane, T.J., Hager, C., and Schroeder, J., 2006, Dynamics of large-magnitude extension in the Whipple Mountains metamorphic core complex: Geochimica et Cosmochimica Acta Supplement, v. 70, p. A616--A616.

Trepmann, C.A., and Seybold, L., 2019, Deformation at low and high stress-loading rates: Geoscience Frontiers, v. 10, p. 43–54, doi:10.1016/j.gsf.2018.05.002.

Tukey, J.W., 1981, Exploratory Data Analysis: Biometrical Journal, v. 23, p. 413–414, doi:10.1002/bimj.4710230408.

Twiss, R.J., 1977, Theory and applicability of a recrystallized grain size paleopiezometer, *in* Pure and Applied Geophysics PAGEOPH, Springer, v. 115, p. 227–244, doi:10.1007/BF01637105.

Wang, P.-L., Lo, C.-H., Chung, S.-L., Lee, T.-Y., Lan, C.-Y., and Van Thang, T., 2000, Onset timing of left-lateral movement along the Ailao Shan--Red River Shear Zone: 40Ar/39Ar dating constraint from the Nam Dinh Area, northeastern Vietnam: Journal of Asian Earth

Sciences, v. 18, p. 281–292.

FIGURE CAPTIONS

TABLE 1. Summary of the experimental conditions and results. Abbreviations: γ, shear strain; τ, shear stress; g.s, grain size; stdev, standard deviation; GOS, grain orientation spread; GCV, geometric coefficient of variation; APR, aspect ratio; NP Skew, non-parametric skew; Skew g.s OL, skew calculated after outliers removed using Tukey's rule (Tukey, 1981); apparent τ, shear stress calculated from recrystallized grains using Cross et al. (2017); Ave τ, the average shear stress calculated over the final 80% of the experiment. Mean grain size and recrystallized grain size are root mean square averages of grain diameters.

Figure 1. A) Mean recrystallized grain size vs. stress from new constant-temperature experiments (black circles) and cooling ramp experiments (squares). Recent EBSD-based calibration of the recrystallized grain size piezometer (black line) and associated constant temperature data (grey circles) from Cross et al. (2017) are also shown. Stress values for ramp experiments are final stresses at the time of quenching. The open circle (W2112) represents an early, non-steady-state condition through which most of the other experiments passed. The arrow on this sample indicates its evolution with strain towards the piezometer (e.g. as demonstrated by W2142). Predicted stress values based on the Hirth et al. (2001) flow law at 800 and 900 °C are in good agreement with the control experiments. For comparison between experiments carried out in different geometries, measured values of shear stress (for general shear) are converted to equivalent stress (e.g., Paterson and Olgaard (2000)), which is equal to differential stress in axial compression (grey circles). Following this conversion, our control experiments plot along the

Cross et al. (2017) piezometer (cf. Heilbronner and Kilian, 2017). Standard errors on grain size are smaller than the plotted symbols. B) Shear stress vs. shear strain for control experiments, and cooling-ramp experiments. Deformation temperatures are given above the mechanical data.
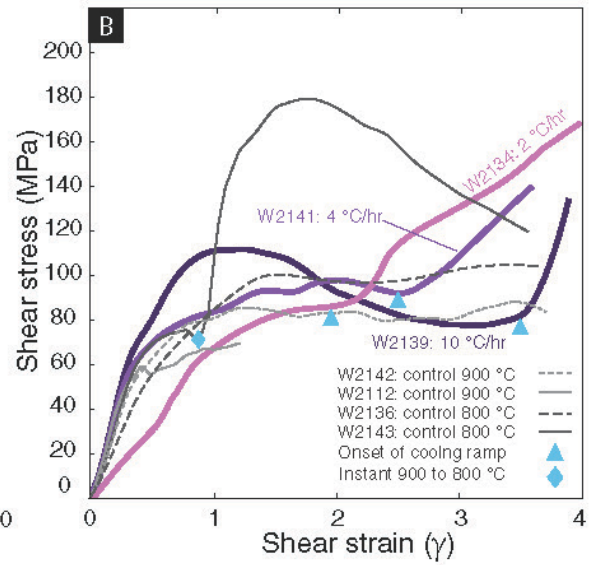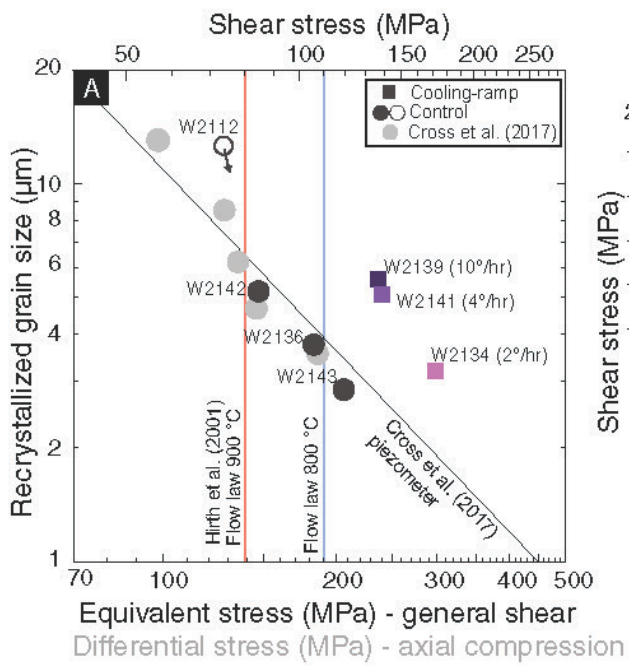

Figure 2. Log-log plot of cooling rate versus shear strain rate for the conducted cooling-ramp experiments and five well-studied naturally-deformed zones. The dashed lines are contours of equal cooling per increment of strain, and suggest an equivalence between the ramp experiments and typical geologic conditions. The beige box represents the ranges of strain-rates and cooling-rates estimated for natural samples. Due to evolution in strain rate and cooling rate with time, considerable variation at each locality is likely, e.g., as shown for the Alpine Fault. "Steady-state" refers to a situation where recrystallized grain size and stress fall along the piezometer (Fig. 1A). Natural data are from Hacker et al. (1992), Foster and John (1999), Wang et al. (2000), Norris and Cooper (2003), Stipp et al. (2004), Stockli et al. (2006), Sassier et al. (2009), Behr and Platt (2011), Kidder et al. (2012, 2013), and Fagereng and Biggs (2018).

Figure 3. A) Probability density functions of normalized grain size for all-grains. The non-dimensional data is generated by taking the log of each measured grain, then dividing each (log) grain size by the mean. Ramp experiments are plotted as thicker, colored lines. The plot demonstrates that fast ramp experiments (4 and 10 °C/hr) have larger concentrations of small grains relative to the other experiments. B) and C) Grain outlines from a ramp experiment (left) and control experiment (right). The scale of the images has been adjusted so that the two images have the same mean grain size. Compared to the control experiment, the ramp experiment has more numerous fine grains and coarse grains, and fewer grains near the mean grain size.
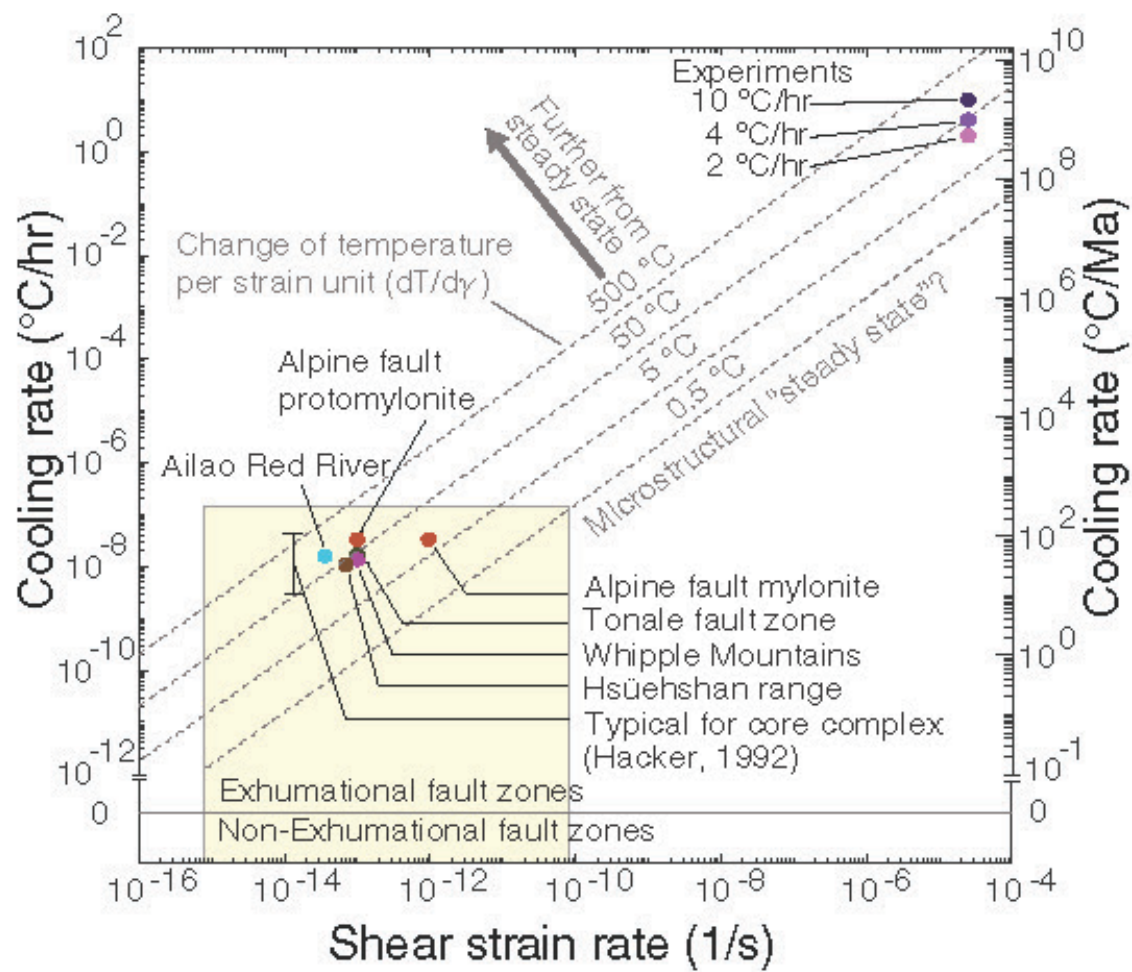
Sample number	W2112	W2142	W2139	W2141	W2134	W2143	W2136
Max T (˚C)	900	900	900	900	900	800	800
Min T (˚C)	-	-	800	800	800	-	-
Cooling rate (˚C/h)	-	-	10	4	2	-	-
Strain, γ	1.2	3.7	3.9	3.5	4.0	3.6	3.6
Final τ (MPa)	74	85	138	140	172	120	106
Ave τ (MPa)	73	82	93	99	108	144	97
Apparent τ (MPa)	51	90	85	89	118	124	107
Number of grains	954	626	796	612	2691	1833	1649
Med. g.s (μm)	12.33	5.31	5.42	5.13	3.33	3.06	3.87
Mean g.s (μm)	15.21	7.03	7.79	7.26	5.10	4.06	5.26
Mean rxld g.s (μm)	13.48	5.39	5.92	5.49	3.49	3.23	4.06
Kurt g.s	6.39	7.44	4.17	5.66	22.55	26.16	9.03
Skew g.s	1.47	1.65	1.19	1.48	3.40	3.44	1.97
Skew g.s OL	0.75	0.79	0.92	0.90	1.01	0.85	0.86
NP skew g.s	0.24	0.22	0.29	0.28	0.29	0.25	0.27
stdev g.s (μm)	6.25	3.52	4.13	3.80	2.92	1.96	2.59
GCV g.s	0.90	0.59	0.67	0.62	0.55	0.45	0.52
Mean GOS (°)	0.76	0.91	1.54	1.30	1.32	0.95	1.07
Median APR	1.57	1.65	1.94	1.66	1.69	1.56	1.75
J-index	1.76	3.49	3.14	3.20	1.95	2.09	3.14

Soleymani et. al., Figure 1., #

Soleymani et. al., Figure 2., #

A

W2142: control 900 °C
W2112: control 900 °C
W2136: control 800 °C
W2143: control 800 °C
W2139: 10 °C/hr
W2141: 4 °C/hr
W2134: 2 °C/hr

PDF

ln(g.s/average g.s)

B

W2139: ramp
10 µm
mean g.s

C
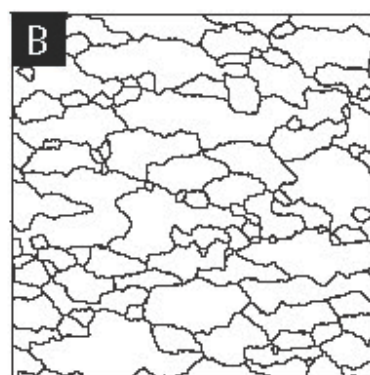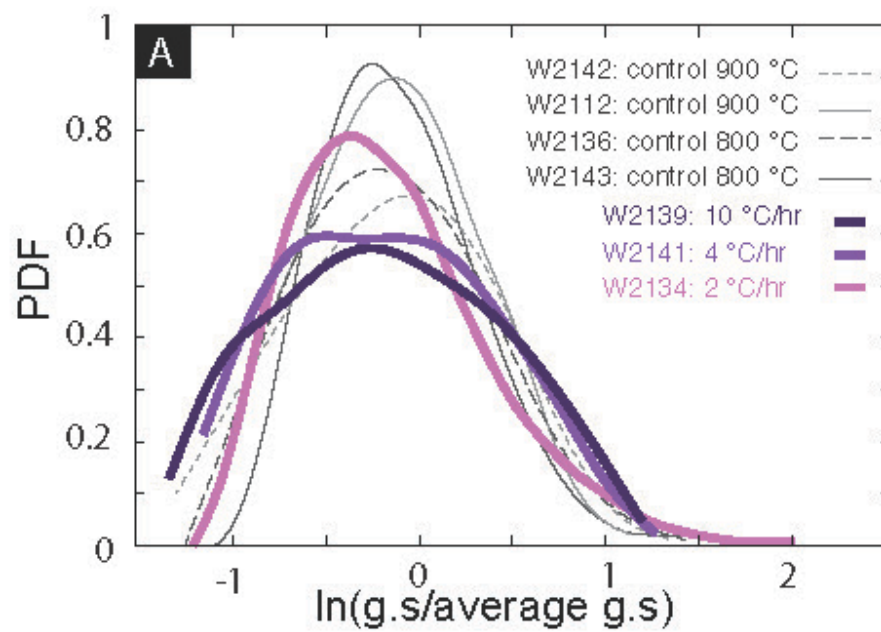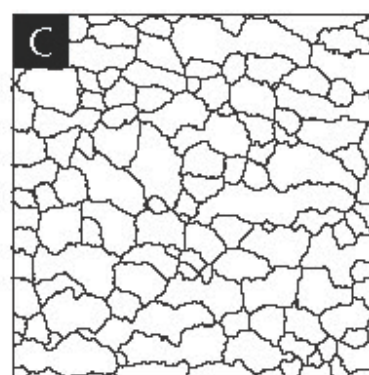
W2143: control
10 µm
mean g.s

Soleymani et. al., Figure 3., #